

Laser oscillation in a highly anisotropic organic crystal with a refractive index of 4.0

Takeshi Yamao,^{a)} Kazunori Yamamoto, Yuki Taniguchi, Tomoharu Miki, and Shu Hotta
*Department of Macromolecular Science and Engineering, Kyoto Institute of Technology,
 Matsugasaki, Sakyo-ku, Kyoto 606-8585, Japan*

(Received 31 January 2008; accepted 4 March 2008; published online 13 May 2008)

We have determined a refractive index of an organic single crystal of a thiophene/phenylene co-oligomer in its laser oscillation wavenumbers. We estimated the refractive index to be 4.0 on the basis of the mode intervals of the well-resolved longitudinal multimodes that are highly polarized along the normal to the (001) plane of the single crystal. This large number is in good agreement with that obtained by the quantum chemical calculations at semiempirical levels. This is also consistent with the high Q factor ($\sim 24\,500$) obtained from the line shape analysis. © 2008 American Institute of Physics. [DOI: [10.1063/1.2919710](https://doi.org/10.1063/1.2919710)]

I. INTRODUCTION

The question of whether the laser oscillation could be achieved in an organic single crystal had remained open since Karl¹ raised it, until Ichikawa *et al.*² affirmatively settled it by observing the laser oscillation from a single crystal of thiophene/phenylene co-oligomer. Since then, several illustrations have been reported on the laser oscillation from the organic single crystals.^{3,4} So far, however, refractive indices, i.e., an important optical constant, have not yet been determined for those crystals.

As molecular crystals usually have a large structural anisotropy, their physical properties are accordingly anisotropic. The anisotropy of both the structure and physical properties is more conspicuous when constituent molecules have a large aspect ratio. This is particularly the case with *oligomers* where several monomer units are linked or fused in terms of organic chemistry. The former is typified by oligothiophenes and oligophenylenes and the latter by pentacene. These molecular materials recently start being applied to electronic devices such as light-emitting diodes⁵ and field-effect transistors.⁶ The oligomer crystals also show interesting optical properties such as spectrally narrowed emissions including, e.g., amplified spontaneous emission^{7,8} and stimulated resonant Raman scattering.⁹ More recently, crystals of specially designed oligomers termed “thiophene/phenylene co-oligomers (TPCOs)” exhibit further intriguing features such as delayed emission.¹⁰ Thus, oligomer crystals are now building up a specific standing among a family of organic semiconductors.

The present studies are pertinent to optical properties of a TPCO crystal. The crystal comprises molecules of 1,4-bis(5-phenylthiophen-2-yl)benzene¹¹ (AC5). In a thin hexagon crystal of AC5, the normal to the wide crystal face [i.e., the (001) plane] is nearly parallel to the molecular long axis with an angle between them being 1.5° .¹² Here, the long axis is defined as a straight line linking the two terminal carbons marked with asterisks [Fig. 1(a)]. This molecular disposition causes the light emission to predominantly take place from the crystal edges,¹³ which indicates that the opti-

cal confinement is effective inside the crystal. Most importantly, the occurrence of a series of well-resolved longitudinal multimodes allows us to unambiguously determine the refractive index of the TPCO crystal.

II. EXPERIMENTS AND COMPUTATION

The AC5 crystal was directly grown in a liquid phase onto a silicon oxide substrate.¹⁴ We carefully selected three different hexagon crystals; see one of them (crystal A) in Fig. 1(b) that gives three different separations defined by three pairs of parallel facets. The individual pair of parallel facets comprises the (010), (110), and ($\bar{1}10$) planes with separations

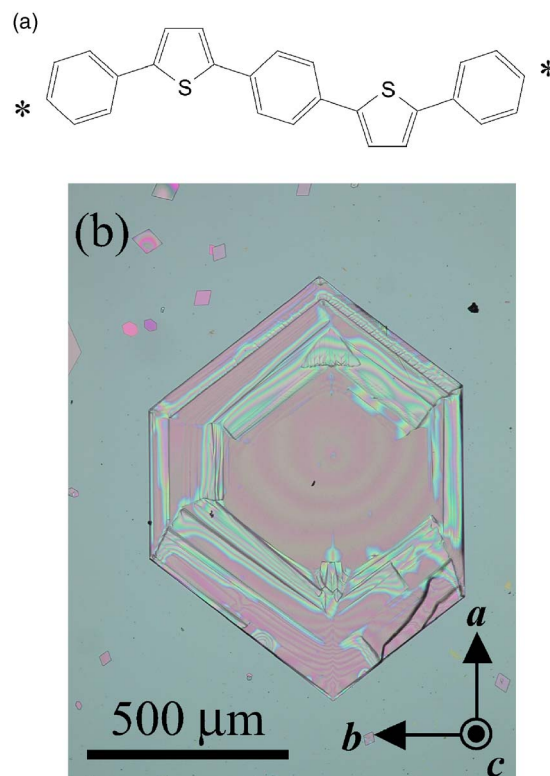


FIG. 1. (Color online) (a) Structural formula of AC5. Its molecular long axis is defined as a straight line linking the two terminal carbons marked with asterisks. (b) Micrograph of the hexagon AC5 crystal.

^{a)}Electronic mail: yamao@kit.ac.jp.

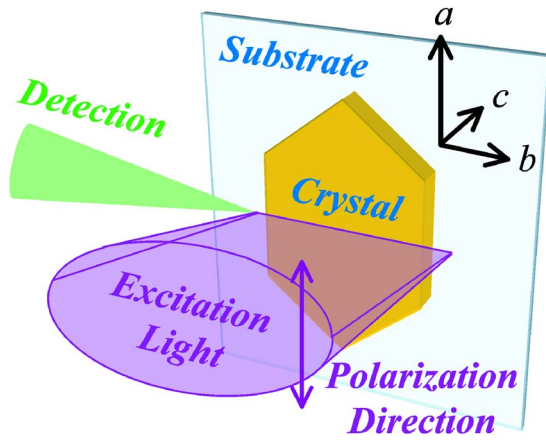


FIG. 2. (Color online) Measurement geometry of the crystal. The laser excitation experiment is being carried out on the pair of parallel (010) facets.

of 789.3, 850.4, and 820.8 μm , respectively. Two other crystals (crystals B and C) are characterized by the separations between the two (010) planes; one was 513.7 μm and the other 788.1 μm . Thicknesses of the crystals ranged from 5.03 to 5.75 μm . We photopumped a thin stripe (~ 50 μm width) of the wide crystal face [the (001) plane] partitioned by the above-mentioned pair of parallel facets. We examined strong emissions occurring from the edges [i.e., the (010), (110), and $(\bar{1}10)$ planes] of that stripe. These emissions are characterized by the longitudinal multimode laser oscillation that takes place between the parallel facets acting as a pair of Fabry–Pérot resonators. In the present studies, we feature the nature of the laser oscillation and demonstrate that it is accompanied by a high refractive index of 4.0.

The measurement geometry of the crystal is shown in Fig. 2, in which the experiment is being carried out on the pair of parallel (010) facets. The experimental setup for the emission measurements is similar to the previous study.¹⁵ Unlike the previous study, however, we used an optical parametric oscillator (LOTIS TII, LT-2215OPO) pumped with a Nd:yttrium aluminum garnet laser (LOTIS TII, LS-2137) for the excitation light source. The excitation wavelength, pulse duration, and pulse repetition rate were 420 nm, 16 ns, and 10 Hz, respectively. The excitation light that is polarized along the fundamental vector a of the space lattice of AC5 crystal was incident perpendicular to the crystal face. The light was focused with a cylindrical lens so as to be a line shape (2 mm in length and 54 μm in width) in parallel with the vector b . The emissions from the crystal were detected along b with a monochromator spectrograph (SOLAR TII, MS7504) equipped with a charge-coupled device camera (Andor, DV401A). For the measurements with the other pairs of facets, the crystal was rotated around the normal to the crystal plane with the excitation polarization retained along a of the crystal.

We carried out the quantum chemical calculations on a MOS-F (Ref. 16) program at a semiempirical level [CNDO/S (Refs. 17 and 18)] to compute the dynamic polarizability tensor. For these calculations, we have borrowed the atomic coordinates from the crystallographic data.¹²

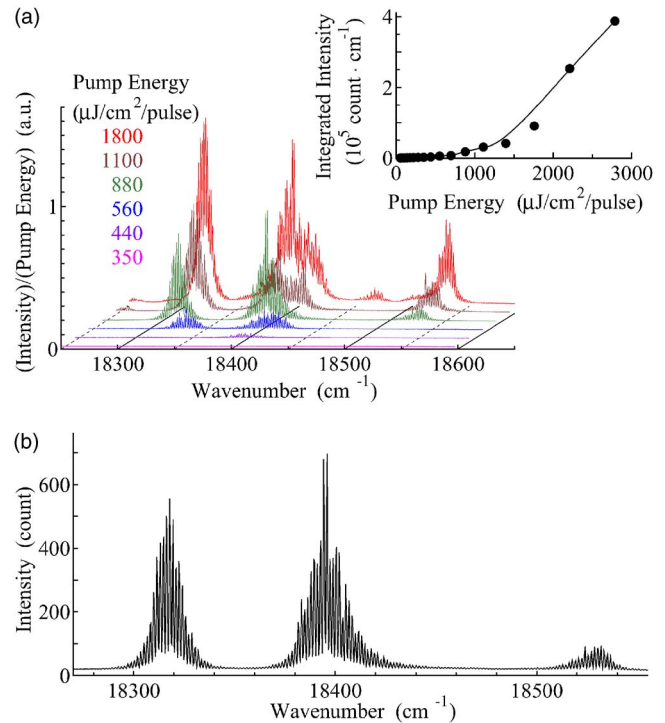


FIG. 3. (Color online) (a) Incident pump energy dependence of spectral profiles of the laser oscillation occurring from the (010) facet of crystal A. The threshold was clearly noted around 440 $\mu\text{J}/\text{cm}^2/\text{pulse}$. Beyond the threshold, equally spaced lines due to longitudinal multimodes are well resolved in the wavenumber region of $\sim 18\,300$ – $18\,550$ cm^{-1} even for weak modes. The inset shows the relationship between the integrated emission intensity and pump energy. (b) Spectral profile taken under an incident pump energy of 880 $\mu\text{J}/\text{cm}^2/\text{pulse}$. The averaged adjacent mode interval for the equally spaced 171 lines was 1.58 cm^{-1} with their standard deviation of 0.169 cm^{-1} .

III. RESULTS AND DISCUSSION

In the previous report,¹⁹ we have shown that the laser oscillation is highly polarized along the normal to the crystal face. The polarization ratio reached ~ 500 , defining that ratio as the emission intensity measured along the normal of the crystal face to that along the direction perpendicular to it.

Figure 3(a) shows the overall spectral profiles of the laser oscillation occurring from the (010) facet of crystal A. The threshold was clearly noted around 440 $\mu\text{J}/\text{cm}^2/\text{pulse}$ (see the inset as well). Beyond the threshold, equally spaced lines are well resolved in the wavenumber region of $\sim 18\,300$ – $18\,550$ cm^{-1} even for weak modes. These lines are due to longitudinal multimodes confined within the pair of the (010) facets. Although the spectral profile started becoming asymmetric beyond 1100 $\mu\text{J}/\text{cm}^2/\text{pulse}$, it recovered an original symmetric profile under weaker excitations. Figure 3(b) depicts an enlarged profile of the spectrum taken under the pump energy of 880 $\mu\text{J}/\text{cm}^2/\text{pulse}$. In Fig. 3(b), the equally spaced multimodes exhibit nearly symmetric profiles centered around 18 320, 18 390, and 18 530 cm^{-1} . Among the equally spaced lines, a series of 171 lines ranged from 18 278.25 to 18 547.66 cm^{-1} , and their averaged adjacent mode interval $\Delta\nu$ was 1.58 cm^{-1} with their standard deviation being 0.169 cm^{-1} .

Once such regular modes are observed, this enables us to determine the refractive index n on the basis of the following expression:

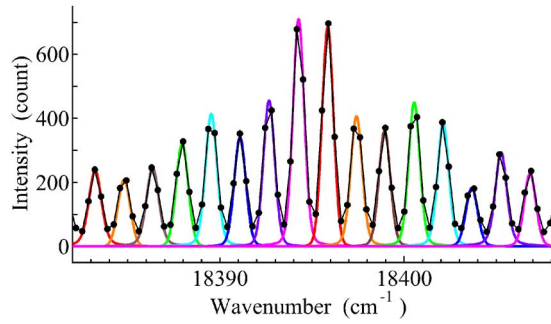


FIG. 4. (Color online) Enlarged profile of the major 16 lines out of the 171 lines mentioned in Fig. 3(b). The black lines and dots indicate the experimental data. The individual lines are fitted with the colored lines produced by modified pseudo-Voigt functions (see text).

$$n = 1/2L\Delta\nu, \quad (1)$$

where L is the separation between a pair of parallel crystal facets. We estimated n to be 4.04 on the basis of the above-mentioned 171 lines. To further confirm the presence of the equally spaced lines, we carried out the line shape analysis on the major 16 lines (out of the 171 lines) around $18\,395\text{ cm}^{-1}$ (see Fig. 4) by using the following modified pseudo-Voigt function:²⁰

$$A \left\{ \eta \exp \left[-4 \ln 2 \left(\frac{\nu - \nu_c}{\nu_w} \right)^2 \right] + \frac{1 - \eta}{4[(\nu - \nu_c)/\nu_w]^2 + 1} \right\}, \quad (2)$$

where A , ν_c , and ν_w represent the height, center location, and full width at half maximum (FWHM) of the peak; η ($0 \leq \eta \leq 1$) is the weight fraction of the Gaussian component on the assumption that the spectral line comprises the Gaussian and the Lorentzian. The fitting function well replicates the original spectrum in such a way that the averaged mode interval $\Delta\nu$ is 1.57 cm^{-1} with their standard deviation of 0.022 cm^{-1} and the averaged FWHM of 0.752 cm^{-1} . The regularity of the equal spacings has been much improved from the decreased standard deviation. The Q factor is estimated at $\sim 24\,500$. We carried out similar measurements on another

TABLE I. Refractive indices of AC5 crystal (crystals A–C). Each number is evaluated by averaging values obtained from Eq. (1).

Sample	Parallel facets	Separation (μm)	Refractive index
Crystal A	(010)	789.3	4.04
	(110)	850.4	4.01
	($\bar{1}10$)	820.8	4.00
Crystal B	(010)	513.7	4.03
Crystal C	(010)	788.1	3.98

two parts of crystal A as well as crystals B and C, confirming the reproducible manifestation of the equally spaced multimodes. The index n ranged from 3.98 to 4.04 (Table I). These numbers are exceptionally high among organic substances.

To justify the high refractive index of AC5, we evaluate the polarizability tensor α_{ij} of the AC5 crystal, where i ($=1, 2$, or 3) stands for the three Cartesian coordinates represented by the unit vectors \hat{a} , \hat{b} , and $\perp ab$ in this order. The vectors \hat{a} and \hat{b} are parallel to the fundamental vectors a and b , respectively.¹² Thanks to the space group symmetry, the polarizability tensor reduces to the following form:

$$\begin{pmatrix} \alpha_{11} & 0 & \alpha_{13} \\ 0 & \alpha_{22} & 0 \\ \alpha_{13} & 0 & \alpha_{33} \end{pmatrix}. \quad (3)$$

Tensor (3) can be readily diagonalized to yield the next matrix if α_{33} dominates other components. (This is the case with the AC5 crystal.)

$$\begin{pmatrix} \alpha_{11} - \alpha_{13}^2/(\alpha_{33} - \alpha_{11}) & 0 & 0 \\ 0 & \alpha_{22} & 0 \\ 0 & 0 & \alpha_{33} + \alpha_{13}^2/(\alpha_{33} - \alpha_{11}) \end{pmatrix}. \quad (4)$$

The corresponding principal refractive index tensor thus takes the following form:

$$\begin{pmatrix} [1 + \alpha_{11} - \alpha_{13}^2/(\alpha_{33} - \alpha_{11})]^{1/2} & 0 & 0 \\ 0 & (1 + \alpha_{22})^{1/2} & 0 \\ 0 & 0 & [1 + \alpha_{33} + \alpha_{13}^2/(\alpha_{33} - \alpha_{11})]^{1/2} \end{pmatrix}. \quad (5)$$

Figure 5 represents the geometrical relationship between the two sets of orthonormal bases (\hat{a} , \hat{b} , and $\perp ab$) and (n_1, n_2 , and n_3). The latter bases are relevant to the three principal axes of the refractive indices and labeled such that n_1 coincides with \hat{b} (the unique axis), obeying the convention for a biaxial crystal.²¹

Two principal axes n_2 and n_3 meet the corresponding two Cartesian axes at an angle θ of approximately 4.2° (see Fig. 5). We obtained 1.50, 1.22, and 3.38 at $18\,395\text{ cm}^{-1}$

(the laser oscillation wavenumber) for the diagonal components of matrix (5). We summarize and compare the computational and experimental results in Table II. Note that the experimentally determined refractive indices associated with a and b (Ref. 12) are the representative numbers below the absorption edge ($14\,300\text{--}20\,000\text{ cm}^{-1}$). The agreement of both the computational and experimental results is pretty good, even though the computed results are systematically smaller than the experimental ones.¹² The polarizability is a rough measure of the spatial extent of the electronic system,

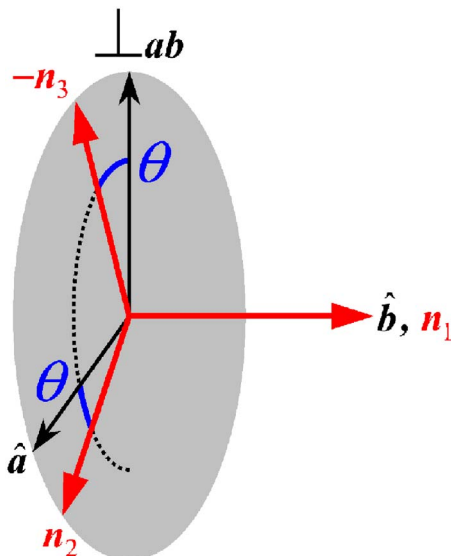


FIG. 5. (Color online) Geometrical relationship between the two sets of orthonormal bases (\hat{a} , \hat{b} , and $\perp ab$) and (n_1 , n_2 , and n_3). The vectors \hat{a} and \hat{b} are parallel to the fundamental vectors of the space lattice for AC5. The latter bases relevant to the principal axes of the refractive indices are produced by rotating the Cartesian axes \hat{a} and $\perp ab$ around \hat{b} by an angle θ . In the present studies, θ was estimated to be 4.2° .

and that extent is by far larger along the molecular long axis than the direction perpendicular to it [see Fig. 1(a)]. A very large refractive index is therefore expected at a wavenumber of the laser oscillation that is predominantly polarized along the normal to the crystal face (i.e., the direction of $\perp ab$).¹⁹ Also, the large refractive index produces a high reflectivity²¹ at the Fabry–Pérot resonators, leading to the high Q factor ($\sim 24\,500$). This number is roughly an order of magnitude larger than that reported for a conducting polymer whose (effective) refractive index is estimated to be around 1.5.²²

IV. CONCLUSION

In conclusion, the well-resolved longitudinal multimode laser oscillations have been observed from the pairs of the

TABLE II. Refractive indices determined by experiments and computations. Experimental results associated with the direction of the vectors a and b are taken from Ref. 12. The number 4.01 is the averaged value listed in Table I. This number is thought to represent the refractive index pertinent to the direction of $\perp ab$ (see text). The computational results represent the diagonal elements of the principal refractive index tensor (5). The orthonormal bases n_1 , n_2 , and n_3 are related to the three principal axes.

	Refractive index		
Experimental	1.87 (a)	1.62 (b)	4.01
Computational	1.50 (n_2)	1.22 (n_1)	3.38 (n_3)

parallel facets of the thin hexagon single crystals of AC5 which were grown in a liquid phase. These oscillations are highly polarized along the normal to the (001) plane of the crystal. From the mode interval of the multimodes, we have demonstrated a very large refractive index of 4.0 for the crystal. By comparing this number to the semiempirically calculated one, we have found out the good agreement between them. This large refractive index is responsible for the high Q factor ($\sim 24\,500$) of the crystals.

ACKNOWLEDGMENTS

This work was supported by a Grant-in-Aid for Science Research in a Priority Area “Super-Hierarchical Structures” (Grant No. 17067009) from the Ministry of Education, Culture, Sports, Science and Technology, Japan.

- ¹N. Karl, *Phys. Status Solidi A* **13**, 651 (1972).
- ²M. Ichikawa, R. Hibino, M. Inoue, T. Haritani, S. Hotta, K. Araki, T. Koyama, and Y. Taniguchi, *Adv. Mater. (Weinheim, Ger.)* **17**, 2073 (2005).
- ³M. Ichikawa, K. Nakamura, M. Inoue, H. Mishima, T. Haritani, R. Hibino, T. Koyama, and Y. Taniguchi, *Appl. Phys. Lett.* **87**, 221113 (2005).
- ⁴K. Shimizu, Y. Mori, and S. Hotta, *J. Appl. Phys.* **99**, 063505 (2006).
- ⁵M. Mazzeo, D. Pisignano, L. Favaretto, G. Barbarella, R. Cingolani, and G. Gigli, *Synth. Met.* **139**, 671 (2003).
- ⁶G. Horowitz, R. Hajlaoui, D. Fichou, and A. E. Kassmi, *J. Appl. Phys.* **85**, 3202 (1999).
- ⁷D. Fichou, S. Delysse, and J.-M. Nunzi, *Adv. Mater. (Weinheim, Ger.)* **9**, 1178 (1997).
- ⁸G. Horowitz, P. Valat, F. Garnier, F. Kouki, and V. Wintgens, *Opt. Mater. (Amsterdam, Neth.)* **9**, 46 (1998).
- ⁹H. Yanagi, A. Yoshiki, S. Hotta, and S. Kobayashi, *Appl. Phys. Lett.* **83**, 1941 (2003).
- ¹⁰F. Sasaki, S. Kobayashi, S. Haraichi, H. Yanagi, S. Hotta, M. Ichikawa, and Y. Taniguchi, *Jpn. J. Appl. Phys., Part 2* **45**, L1206 (2006).
- ¹¹S. Hotta, H. Kimura, S. A. Lee, and T. Tamaki, *J. Heterocycl. Chem.* **37**, 281 (2000).
- ¹²T. Yamao, Y. Taniguchi, K. Yamamoto, T. Miki, S. Ota, S. Hotta, M. Goto, and R. Azumi, *Jpn. J. Appl. Phys., Part 1* **46**, 7478 (2007).
- ¹³T. Yamao, K. Yamamoto, Y. Taniguchi, and S. Hotta, *Appl. Phys. Lett.* **91**, 201117 (2007).
- ¹⁴T. Yamao, T. Miki, H. Akagami, Y. Nishimoto, S. Ota, and S. Hotta, *Chem. Mater.* **19**, 3748 (2007).
- ¹⁵T. Yamao, T. Ohira, S. Ota, and S. Hotta, *J. Appl. Phys.* **101**, 083517 (2007).
- ¹⁶A. Matsuura, *MOS-F Version 6.0A* (Fujitsu, Tokyo, 2003).
- ¹⁷J. D. Bene and H. H. Jaffé, *J. Chem. Phys.* **48**, 1807 (1968).
- ¹⁸R. L. Ellis, G. Kuehnlenz, and H. H. Jaffé, *Theor. Chim. Acta* **26**, 131 (1972).
- ¹⁹T. Yamao, K. Yamamoto, T. Miki, H. Akagami, Y. Nishimoto, and S. Hotta, *Phys. Status Solidi C* (in press).
- ²⁰K. Heinze, K. Hempel, and M. Beckmann, *Eur. J. Inorg. Chem.* **2006**, 2040 (2006).
- ²¹A. Yariv and P. Yeh, *Optical Waves in Crystals: Propagation and Control of Laser Radiation* (Wiley, Hoboken, NJ, 2003).
- ²²S. V. Frolov, M. Shkunov, Z. V. Vardeny, and K. Yoshino, *Phys. Rev. B* **56**, R4363 (1997).